J. Phys.: Condens. Matter 6 (1994) 5761–5770. Printed in the UK

Anisotropy of the photoelectron mean free path and its influence on the EXAFS amplitude

Alexei Kuzmin
Institute of Solid State Physics, University of Latvia, LV-1063 Riga, Latvia

Received 12 October 1993, in final form 18 April 1994

Abstract. The anisotropy of the inelastic mean free path (MFP) for electrons with energies between ~10–1000 eV has been studied for the first time in ReO_3, $NaWO_3$ and TiO crystals. The MFP was calculated within the one-plasmon and local density approximations from the imaginary part of the complex energy-dependent exchange and correlation potential of the Hedin–Lundqvist type. It is shown that the MFP in compounds with a highly anisotropic electron density distribution, such as ReO_3 and $NaWO_3$, differs in various crystallographic directions from the MFP calculated for the averaged electron density. In particular, it was found that in the ReO_3 crystal, the MFP values in ⟨100⟩ directions coincide with those for a spherically averaged cluster potential and are ~ 1 Å smaller than in ⟨110⟩ and ⟨111⟩ directions. This result explains the variation of the outer shell amplitudes in the Re L_3-edge EXAFS in ReO_3.

1. Introduction

The inelastic mean free path (MFP) plays an important role in x-ray absorption spectroscopy (XAS), as in almost any experiment in which the excited electron moves through a solid, for example Auger, electron energy loss and x-ray photoemission spectroscopies, low-energy electron diffraction, etc. However, the experimental data for a given compound are usually available in an extremely limited energy range and, moreover, have a great degree of uncertainty due to associated experimental difficulties [1–3]. From the theoretical point of view, the MFP $\lambda(E)$ can be calculated using either a purely phenomenological theory derived from a general behaviour of MFP in different materials [3], or statistical theory [2, 4–6]. The phenomenological theory is based on approximating existing experimental data by the simple form $\lambda(E) = AE^{-2} + BE^{1/2}$, where A and B are fitting parameters [3]. The statistical approach is based on the assumption that the inelastic scattering of an electron in a small volume of the solid can be approximated by the scattering appropriate to a free-electron gas of electron density $\rho(r)$, in the same volume [4]. It was successfully applied to several *free-electron-like* compounds and gave the MFP values that agree well with known experimental results [2, 6]. Both approaches are currently widely used in the analysis of the XAS data [7–10].

In x-ray absorption spectra, the inelastic MFP leads to exponential amplitude damping of the extended x-ray absorption fine structure (EXAFS) beyond the absorption edge, and limits a region around the absorber in which located atoms contribute in EXAFS [7]. A precise knowledge of MFP is needed to obtain other amplitude-related parameters, such as coordination numbers and Debye–Waller factors [7]. Moreover, the dependence of MFP on electron density can in some cases make doubtful the possibility of transferability of scattering amplitudes and phases from one compound to another, often used at present in EXAFS analysis.

0953-8984/94/295761+10$19.50

The general approach to the calculation and interpretation of EXAFS spectra is based currently on the *multiple-scattering* (MS) formalism utilizing a *complex optical* potential within statistical exchange and *muffin-tin* (MT) approximations [10]. In such an approach, the potential is spherically averaged around each atom and volume averaged in the interatomic (interstitial) region. As a result, the inelastic MFP of the exited electron is *isotropic*. Recently it was noted [7] that, in reality, the losses due to the electron–electron interaction cannot always be described by an isotropic MFP, particularly for covalently bonded solids, in which the valence charge distribution is directional; therefore, further studies are required to estimate the magnitude of correction due to the effect of anisotropy.

In the present work the anisotropy of the inelastic MFP in ReO_3, $NaWO_3$ and TiO crystals is studied for the first time within the statistical approximation, which should be a good approach since all three compounds have metallic conductivity [11]. The origin and magnitude of the MFP anisotropy, found in the ReO_3 crystal and supported by the results of the Re L_3-edge EXAFS analysis, is discussed and compared to other compounds.

2. Theory

We present below a brief description of the theoretical background for the inelastic MFP calculation and its relation to EXAFS. Atomic units ($\hbar = m = e = 1$) will be used throughout this section.

The normalized EXAFS-signal $\chi(E)$ is related to the absorption coefficient $\mu(E)$ by the expression [12]

$$\chi(E) = \big(\mu(E) - \mu_0(E)\big)/\mu_0(E) \tag{1}$$

where μ_0 is the atomic absorption coefficient in the absence of neighbouring atoms (it is usually a smooth function). In the *dipole* and *one-electron* approximations, the absorption coefficient μ is given by [13, 14]

$$\mu \sim \sum_k |\langle \phi_k | \hat{\epsilon} \cdot r | \phi_{k'} \rangle|^2 S_0^2 \tag{2}$$

where ϕ_k is the one-electron final-state wavefunction of the excited electron (the photoelectron) with momentum k in the presence of the core-hole, $\phi_{k'}$ is the one-electron atomic-like initial-state wavefunction and $\hat{\epsilon}$ is the x-ray polarization vector. The S_0^2 factor ($S_0^2 < 1$) describes the amplitude reduction due to the *intrinsic* multielectron excitations [13, 14], and the calculations done within different approximations show that S_0^2 lies in the range 0.8–1.0 [13].

The many-body interactions between the excited electron and other electrons, leading to the *extrinsic* losses, are taken into account in the *one-electron* approximation (equation (2)) through an appropriate *complex optical* potential, which has Coulomb $V(r)$ and exchange-correlation $V_{xc}(r)$ parts [13]. In this case, the final-state wavefunction $\phi_k(x)$ of a photoelectron satisfies a Schrödinger-like equation [15]

$$\left(-\tfrac{1}{2}\nabla^2 + V(r) - E_k\right)\phi_k(x) + \int \Sigma(x, x'; E_k)\phi_k(x')\,dx' = 0 \tag{3}$$

where x denotes both the space coordinate and spin, $x = (r, s)$, and Σ is a *non-local* complex energy-dependent potential describing exchange and correlation effects. If the charge density of the system $\rho(r)$ is a slowly varying function compared to the local

de Broglie wavelength ($\lambda = 2\pi/k$) then in the *local density* approximation (LDA), according to Sham and Kohn [16]

$$\int \Sigma(x, x'; E_k)\phi_k(x')\,dx' \simeq \Sigma_h\big(p(r); E_k - V(r); \rho(r)\big)\phi_k(x) \tag{4}$$

where Σ_h is the self-energy of a photoelectron with momentum $p(r)$ and energy $E(p, \rho) = E_k - V(r)$ in a homogeneous electron gas of density $\rho(r)$. Following Lee and Beni [17], the self-energy Σ_h can be further approximated using the Thomas–Fermi description of an atom:

$$\Sigma_h\big(p(r); E_k - V(r); \rho(r)\big) \simeq \Sigma_h\big(p(r); \tfrac{1}{2}p^2(r)\big) \equiv V_{xc}(r). \tag{5}$$

The lifetime of an electron with energy $E_k = k^2/2$ and momentum k propagating in a free-electron gas of density ρ is equal to $(2\,\mathrm{Im}\Sigma_h)^{1/2}$, and its MFP $\lambda(E, \rho)$ is given by [5, 6, 18]

$$\lambda(E, \rho) = -\frac{k}{2\,\mathrm{Im}\Sigma_h(\mathrm{E}, \rho)}. \tag{6}$$

In the photoabsorption process, the lifetime of a photoelectron is additionally limited by the presence of the core-hole, and the effective MFP can be introduced in this case [9]:

$$\lambda_{eff}(E, \rho) = \frac{k}{\Gamma_{CH} - 2\,\mathrm{Im}\Sigma_h(\mathrm{E}, \rho)} \tag{7}$$

where Γ_{CH} is the full width of the core-hole level [19]. In Hartree–Fock theory, the electron self-energy Σ_h is related to the dielectric function $\epsilon(q, \omega)$ and can be found using the Lindhard theory of screening, also known as the *random-phase* approximation (RPA) [4, 18]. Within this approach, the extrinsic losses arise due to the excitation of plasma oscillations by the photoelectron [18]. However, it was shown [5, 15] that further simplification based on the *one-pole* approximation for the dielectric function can be used without significant loss of accuracy. In this work, the imaginary part of the photoelectron self-energy was calculated using the analytical formula given in [9].

Table 1. Structural data for the calculation of the cluster potentials. (a is the lattice parameter, R_{MT} the muffin-tin radius and ρ_{ave} the average electron density.)

	Cu	Au	ReO_3	$NaWO_3$	TiO
a (Å)	3.615	4.079	3.750	3.860	4.1766
R_{MT} (Å)	1.30	1.47	1.06 (Re) 1.00 (O)	1.10 (W) 1.03 (O) 1.03 (Na)	1.27 (Ti) 1.05 (O)
Overlap (%)	1.7	2	10	10	10
ρ_{ave} (electrons Å^{-3})	2.456	4.657	1.877	1.895	1.647
Edge	K-Cu	L_3-Au	L_3-Re	L_3-W	K-Ti

The electron density for the compound of interest in a given direction as a spherically averaged cluster density were calculated using the MSCALC code [8]. The cluster, including all atoms inside a sphere of radius 8 Å centred at the absorber, was used and its potential was constructed from a set of overlapped MT potentials using structural data presented in table 1. The MT potentials were built according to the following procedure: the atomic charge

densities obtained from self-consistent solutions of the Dirac equations were placed on each atomic site in the cluster, and the superposed charge density was averaged *spherically* or in a *solid angle* about the central atom (absorber). The total number of electrons in the whole cluster was the same as in the real compound; therefore, in the case of *spherical* averaging, the average electron density ρ_{ave} corresponds to the one in the real system (table 1). In the case of the averaging in a *solid angle*, it differs for different crystallographic directions depending on the compound. In particular, for the ReO_3 crystal the average electron density in ⟨100⟩ directions, coinciding with Re–O bonds, is greater than in ⟨110⟩ and ⟨111⟩ directions. Furthermore, the complex energy-dependent exchange-correlation potential (ECP) of Hedin–Lundqvist (HL) type [9] was calculated from the averaged electron density, and the MFP was found from the imaginary part of the HL ECP according to (6) and (7).

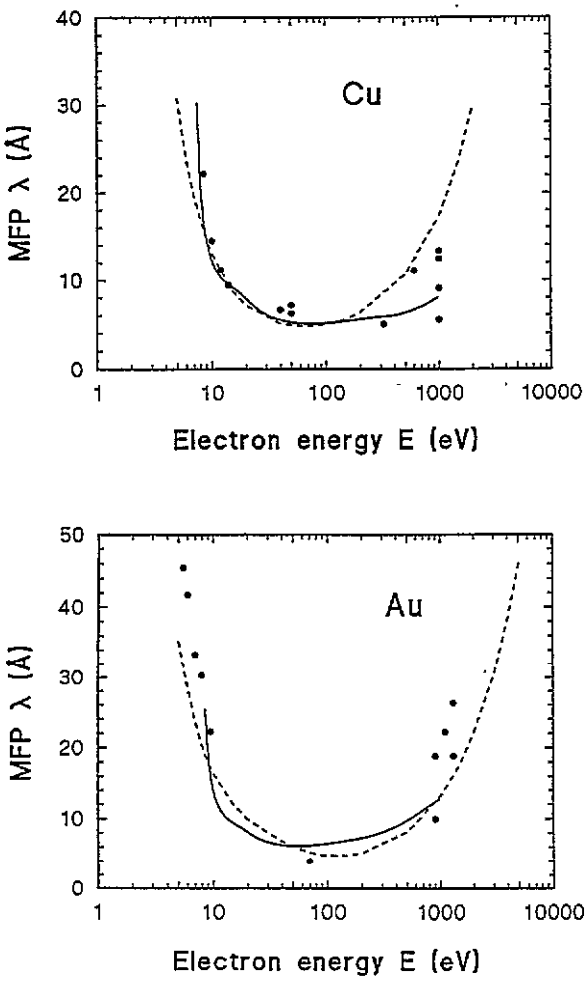

Figure 1. Inelastic MFP $\lambda(E)$ of the photoelectron in copper and gold, calculated for a spherically averaged cluster potential in the present work (full curves) from the imaginary part of the complex Hedin–Lundqvist potential for the Cu K edge and Au L_3 edge, in comparison with experimental data (full circles) taken from [2, 6]. The broken curves show Penn's calculations [6].

To illustrate the accuracy of the approach used, the MFPs calculated for copper and gold in this work are shown in figure 1 in comparison with experimental data taken from [2, 6] and the calculations of Penn [6] based on a model dielectric function. The agreement between the present results and experimental data is good enough. However, some deviation from Penn's results for copper at high energies is present. This may be due to the fact that

calculations of MFP in [6] are based on experimentally measured dielectric functions, while in the present work they were calculated as suggested in [13].

The influence of MFP on the EXAFS amplitude is clear from the analytical expression for $\chi(k)$. In the *multiple-scattering* approach [10], the oscillating structure of the absorption coefficient $\chi(k)$, given by (1), has the general form

$$\chi(k) = \sum_n A_n(k, R_n^{ij}) \sin\left(kR_n + \Phi_n(k, R_n^{ij})\right) \tag{8}$$

where the sum is taken over all possible closed paths, $\Phi_n(k, R_n^{ij})$ is the effective scattering phase, R_n is the total path length and R_n^{ij} is the length of the path from atom i to atom j. The term $A_n(k, R_n^{ij})$ is the effective scattering amplitude, which depends on (i) the scattering path degeneracy N_n equal to the coordination number for the single-scattering paths, (ii) the Debye–Waller factor (DWF) σ_n^2, entering through the term $\exp(-2\sigma_n^2 k^2)$, reflecting both static and thermal disorder effects, and (iii) the MFP $\lambda_n(k)$, entering through the term $\exp\left(-R_n/\lambda_n(k)\right)$. The MFP is a function of electron density (see (6) and (7)), whose distribution in a compound can be anisotropic (in particular, the electron density is higher when two atoms in a scattering path are chemically bonded); therefore $\lambda_n(k)$ differs in the general case for different geometrical paths of the photoelectron, and thus for different MS signals generated within a cluster. All three parameters (N_n, σ_n^2 and $\lambda_n(k)$), containing in $A_n(k, R_n^{ij})$, are highly correlated, particularly DWF and MFP since their influence on the EXAFS amplitude is similar (exponential-like). Therefore, the precise determination of structural parameters requires accurate information on MFP. In this work, for simplicity, we will consider only the variations of $\lambda_n(k)$ (denoted below as $\lambda(k)$) corresponding to the single-scattering (SS) signals from atoms which are located in different crystallographic directions from the absorber. In this case, $\lambda(k)$ can be simply calculated from the imaginary part of the self-energy based on the interatomic charge-density distribution according to the procedure described before. As a result, one can expect qualitatively that the value of $\lambda(k)$ will be the smallest along the directions of chemical bonds where the electron density is the highest. For the systems ReO_3, $NaWO_3$ and TiO this corresponds to the ⟨100⟩ directions. However, the numerical estimate of differences in $\lambda(k)$ for three main crystallographic directions ⟨100⟩, ⟨110⟩ and ⟨111⟩, corresponding, in the case of ReO_3, for example, to the SS signals from rhenium atoms in the second, fourth and sixth coordination shells, is of great interest.

3. Results and discussion

The anisotropy of the electron density distribution is closely related to the crystallographic structure of the material; therefore, the three compounds considered in this work were chosen according to the following criteria. (i) Their structures consist of highly covalent metal–oxygen bonds and show a transition from the open perovskite-like structure (ReO_3) to the perovskite structure ($NaWO_3$) and to the close-packed sodium chloride structure (TiO); therefore, the anisotropy of the electron density around the metal ion decreases from ReO_3 to TiO. (ii) The statistical approach to the electron self-energy should be good approximation in ReO_3, $NaWO_3$ and TiO, since all three compounds have metallic conductivity [11].

A typical Fourier transform (FT) of the Re L_3-edge EXAFS $\chi(k)k^2$ in ReO_3, taken from [20], is shown in figure 2. Note that the FT has not been corrected on the photoelectron phase shift $\Phi_n(k, R_n^{ij})$ (see equation (8)), and therefore the positions of peaks in figure 2 differ from the true crystallographic values. There are five peaks in the range up to 7 Å,

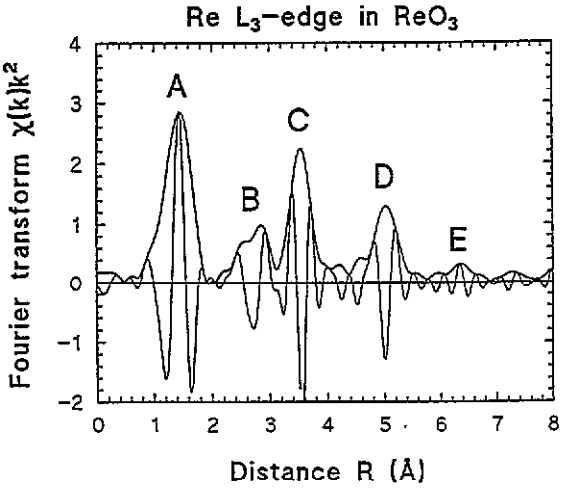

Figure 2. Fourier transform (FT) of the experimental Re L_3 edge EXAFS spectrum $\chi(k)k^2$ in ReO_3 (both modulus and imaginary parts of FT are shown). Data are taken from [20]. The main peaks discussed in the text are labeled.

labeled A, B, C, D and E, whose origin was described in detail in [20]. Here we will be interested only in the final three peaks C, D and E related to coordination shells formed mainly by rhenium atoms. Peak C is attributed to the second shell containing six rhenium atoms ($N_C = 6$) located along crystallographic axes in ⟨100⟩ directions at $R_C = 3.75$ Å. Its amplitude is enlarged due to a strong focusing effect caused by the oxygen atoms of the first shell [20]. Peak D corresponds mainly to twelve rhenium atoms ($N_D = 12$) located in ⟨110⟩ directions at a distance $R_D = 5.30$ Å, and peak E is due to eight rhenium atoms ($N_E = 8$) in ⟨111⟩ directions at $R_E = 6.50$ Å. One can see that the first four peaks (A–D) are well defined, whereas the amplitude of the last peak E decreases abruptly by a factor of about four, compared to the previous peak D, despite the expected value of a factor of about two, roughly estimated as $(N_D/R_D^2)/(N_E/R_E^2)$. Note that, owing to the large values of the distances R_D and R_E, the differences in the scattering amplitudes, due to spherical corrections and, in Debye–Waller factors [21], due to a correlation of motion of rhenium atoms, are negligible. The number of well resolved peaks in FT was related recently to the cluster dimension defining only atoms around the absorber that can make a significant contribution to the EXAFS spectrum [20]. The cluster dimension was roughly estimated from the effective MFP calculated for a spherically averaged cluster potential (see figure 2(*a*) in [20]); however, a precise analysis shows that the values of the MFP, lying in the range 3 Å to ~ 5 Å [20], are small enough, and one can expect that the amplitude of the peak D should decrease abruptly. This is the reason why the calculation, carried out in [20], gives an understated amplitude of the peak D.

It is known that rhenium trioxide is characterized by highly anisotropic vibrational properties related to very strong rhenium–oxygen bonds in ⟨100⟩ directions [21], whose presence is confirmed by the anisotropic charge distribution around rhenium atoms determined by an x-ray structural analysis (see figures 1 and 2 in [22]). A simplified electron density diagram for ReO_3, calculated in the MT approximation as the sum of atomic electron densities, and its contour plot in the (001) plane, are shown in figure 3. One can see that the electron density along the crystallographic axes is large compared to that in ⟨110⟩ or ⟨111⟩ (not shown) directions. The MFP calculated along three directions, as for a spherically averaged cluster potential, according to the approach described in section 2, is shown in figure 4. The error bar in figure 4(*b*) represents the range in which a shift of the effective MFP curves can take place, due to inaccuracies of the core-level width values reported in the literature. It is clearly visible that across faces and along diagonals of the

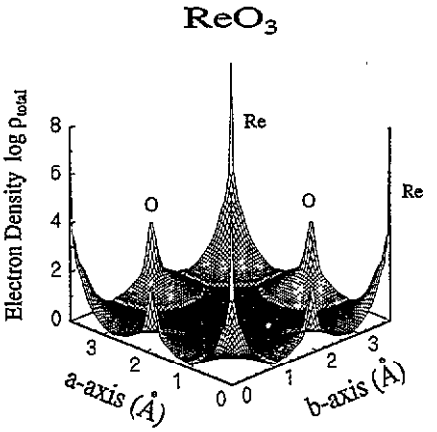

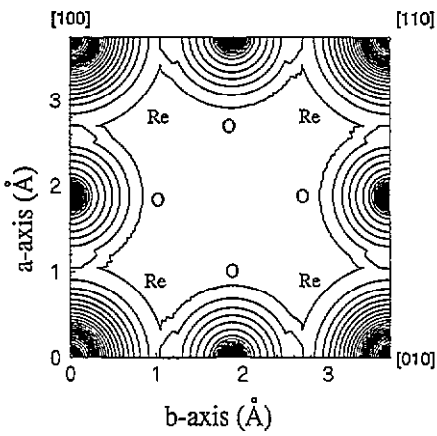

Figure 3. Total electron density ρ_{total} in the (001) plane of ReO_3 crystal obtained as the sum of atomic electron densities calculated in the muffin-tin approximation.

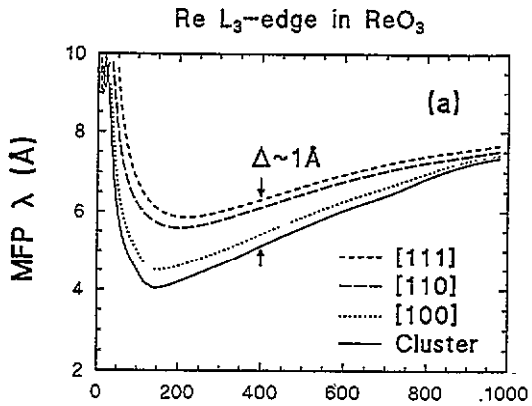

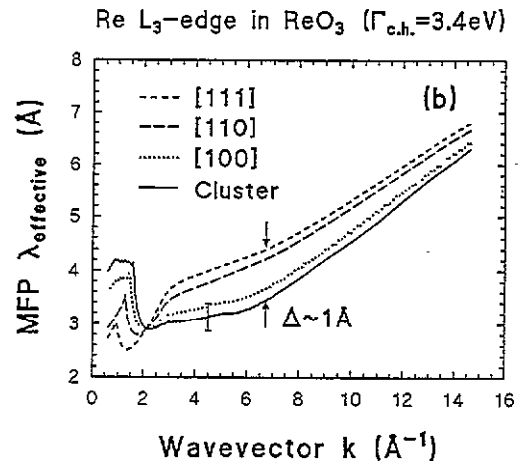

Figure 4. (*a*) Inelastic MFP $\lambda(E)$ calculated from the imaginary part of the complex Hedin–Lundqvist potential for the Re L_3 edge in ReO_3 in three crystallographic directions ([100], [110] and [111]) and for a spherically averaged cluster potential. (*b*) Effective MFP $\lambda_{eff}(E)$ taking into account the core-level width of the Re L_3-edge $\Gamma_{CH} = 3.4$ eV [19].

cubic unit cell of ReO_3, in ⟨110⟩ and ⟨111⟩ directions, respectively, the MFP has similar values, which are about 1 Å larger than along ⟨100⟩ directions and for a spherically averaged cluster potential. This difference explains (i) the presence of a well defined peak D, (ii) the disagreement in its amplitude between the calculation of [20] and experiment and (iii) the abrupt decrease of the E-peak amplitude. The numerical results show that, due to the difference between the MFP value, calculated for a spherically averaged potential, and that in the ⟨110⟩ directions, the amplitude of the EXAFS signal, related to the peak D and calculated in [20], should be multiplied by the energy-dependent coefficient having values in the range 1.25–2.0 which improves the agreement with experiment. Furthermore, small differences in the MFP values in ⟨110⟩ and ⟨111⟩ directions are responsible for an additional increase in the

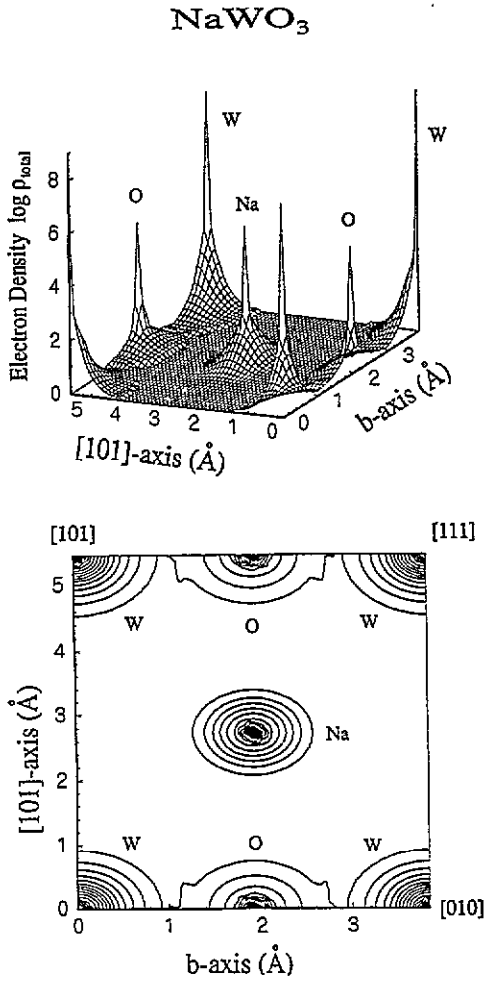

Figure 5. Total electron density ρ_{total} in the $(10\bar{1})$ plane of an $NaWO_3$ crystal obtained as the sum of atomic electron densities calculated in the muffin-tin approximation.

ratio of amplitudes of the peak D to the peak E, which is about four times that of experiment (figure 2). As was pointed out above, the contribution to this ratio from the difference in coordination numbers and distances is about two. Due to the MFP anisotropy, it becomes about 1.2–1.4 times greater. The remaining difference can be explained by the additional contribution in the peak D of 30 oxygen atoms located at 5.6 Å. Thus, the anisotropy of the MFP in ReO_3 leads to changes of the outer-shells EXAFS amplitude up to 60%.

$NaWO_3$ has a modified ReO_3 structure with a slightly increased lattice parameter (table 1) and sodium ions located in the centre of the cubes formed by eight $W^{5+}O_6$ octahedra. The electron distribution in the (001) plain of $NaWO_3$ is similar to ReO_3 but, in the $(10\bar{1})$ plane, it differs due to the presence of sodium atoms (figure 5). Since tungsten W^{5+} and rhenium Re^{6+} ions have similar electronic structures, the modification of the MFP in the ⟨100⟩ and ⟨110⟩ directions in $NaWO_3$ compared to ReO_3 is mainly due to the increase of the lattice parameter leading to the decrease of electron density in these directions and to the increase of MFP. However, in the ⟨111⟩ directions, where sodium atoms are located halfway between two tungsten ions, the charge density increases and, respectively, the MFP decreases (figure 6).

The close-packed structure of titanium oxide results in quasi-spherically symmetric

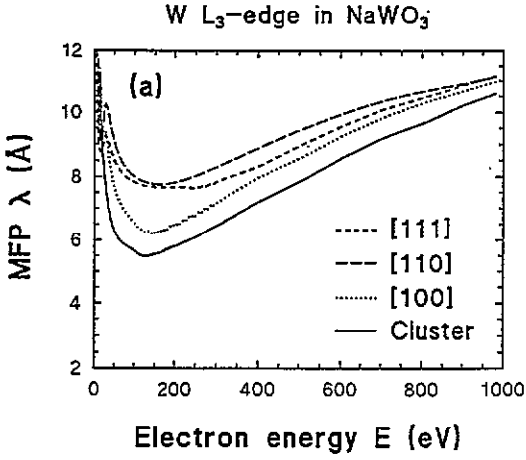

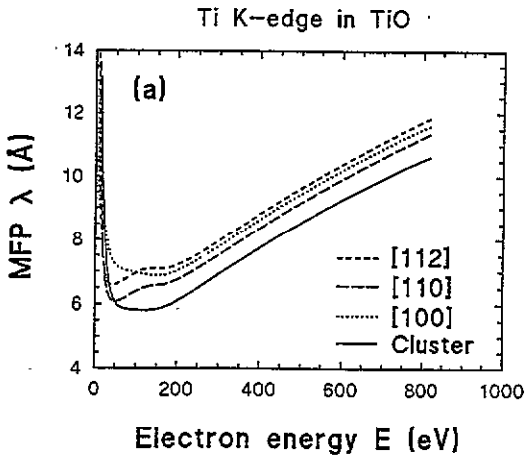

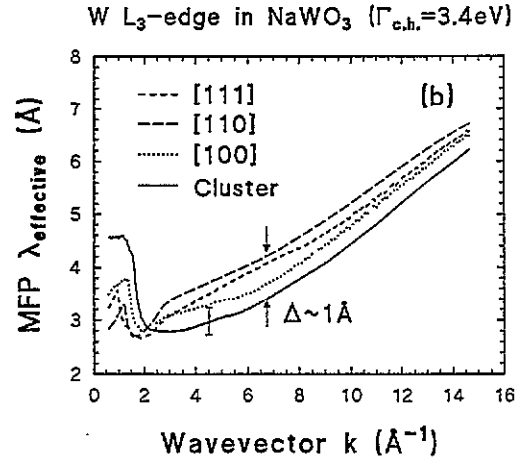

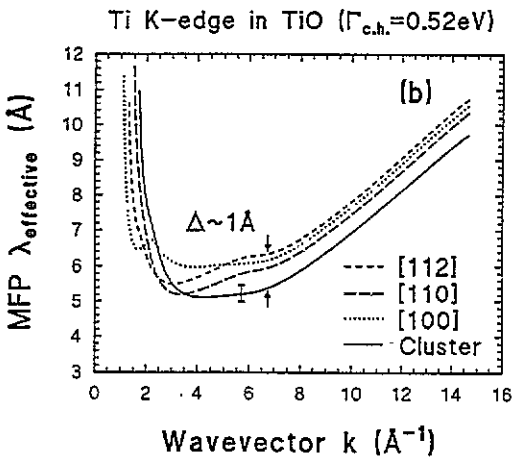

Figure 6. (*a*) Inelastic MFP $\lambda(E)$ calculated from the imaginary part of the complex Hedin–Lundqvist potential for the W L_3 edge in $NaWO_3$ in three crystallographic directions ([100], [110] and [111]) and for a spherically averaged cluster potential. (*b*) Effective MFP $\lambda_{eff}(E)$ taking into account the core-level width of the W L_3 edge $\Gamma_{CH} = 3.4$ eV [19].

Figure 7. (*a*) Inelastic MFP $\lambda(E)$ calculated from the imaginary part of the complex Hedin–Lundqvist potential for the Ti K edge in TiO in three crystallographic directions ([100], [110] and [112]) and for a spherically averaged cluster potential. (*b*) Effective MFP $\lambda_{eff}(E)$ taking into account the core-level width of the Ti K edge $\Gamma_{CH} = 0.52$ eV [19].

charge distribution around titanium ions. The MFP calculated in the ⟨100⟩, ⟨110⟩ and ⟨112⟩ directions corresponding to the directions of nearest-neighbour metal ions, which produce the main contribution in EXAFS, are shown in figure 7. As was expected, their values are close to each other, reflecting the isotropic character of the electron density around titanium. It is also necessary to note that the MFP along ⟨100⟩ directions, which correspond in the studied compounds to the metal–oxygen–metal linear chains, is close to the MFP for a spherically averaged cluster potential in ReO_3 and becomes slightly larger in TiO. This fact may be the reason for the incorrect values of the EXAFS amplitude for the second shell of titanium ion when the conventional approach, based on a spherically averaged cluster potential, is used [8, 10].

4. Conclusions

In the present work the anisotropy of the inelastic mean free path (MFP) for electrons with energies between ~10 and 1000 eV was studied for the first time in ReO_3, $NaWO_3$ and TiO crystals. The MFP was calculated within the statistical approximation from the imaginary part of the complex energy-dependent exchange and correlation potential of Hedin–Lundqvist type. It is found that, in the presence of the anisotropy of the charge distribution, the MFP values differ considerably in various crystallographic directions compared to the MFP for a spherically averaged cluster potential. This effect should be of great importance, particularly in covalently bonded solids with an open structure. Furthermore, as is shown in the example of the Re L_3-edge EXAFS, the anisotropy of the MFP leads to significant changes (up to 60%) in the outer-shells EXAFS amplitude.

Acknowledgments

The author is grateful to Dr T A Tyson (Stanford University) for helpful and valuable discussions. He wishes to thank Professors C R Natoli and M Benfatto (Laboratori Nazionali di Frascati) and Dr T A Tyson for the possibility of using their MSCALC code. Friendly and stimulating discussions with Dr E-D Klinkenberg (Rostock Universität) and the hospitality of the Università di Trento (Professor G Dalba and Dr F Rocca), where part of this work was done, are also acknowledged.

References

[1] Powell C J 1974 *Surf. Sci.* **44** 29
[2] Tung C J, Ashley J C and Ritchie R H 1979 *Surf. Sci.* **81** 427
[3] Seah M P and Dench W A 1979 *Surf. Interface Anal.* **1** 2
[4] Lindhard J 1954 *Kgl. Dansk. Vidensk. Selsk. Mat.-Fys. Med.* **28** No 8
[5] Penn D R 1976 *Phys. Rev.* B **13** 5248
[6] Penn D R 1987 *Phys. Rev.* B **35** 482
[7] Stern E A 1988 *X-ray Absorption: Principles, Applications, Techniques of EXAFS, SEXAFS and XANES* ed D C Koningsberger and R Prins (New York: Wiley)
[8] Ruiz-Lopez M F, Loos M, Goulon J, Benfatto M and Natoli C R 1988 *Chem. Phys.* **121** 419
Tyson T A 1991 *PhD Thesis* University of Stanford
[9] Mustre de Leon J, Rehr J J, Zabinsky S I and Albers R C 1991 *Phys. Rev.* B **44** 4146
[10] Tyson T A, Hodgson K O, Natoli C R and Benfatto M 1992 *Phys. Rev.* B **46** 5997
[11] Goodenough J B 1971 *Prog. Solid State Chem.* **5** 145
[12] Lee P A and Pendry J B 1975 *Phys. Rev.* B **11** 2795
[13] Chou S-H 1982 *PhD Thesis* University of Washington
Chou S-H, Rehr J J, Stern E A and Davidson E R 1987 *Phys. Rev.* B **35** 2604
[14] Rehr J J, Stern E A, Martin R L and Davidson E R 1978 *Phys. Rev.* B **17** 560
[15] Hedin L 1965 *Phys. Rev.* **139** A796
Hedin L and Lundqvist S 1969 *Solid State Phys.* **23** 1
Hedin L and Lundqvist S 1971 *J. Phys. C: Solid State Phys.* **4** 2064
[16] Sham L J and Kohn W 1966 *Phys. Rev.* **145** 561
[17] Lee P A and Beni G 1977 *Phys. Rev.* B **15** 2862
[18] Quinn J J 1962 *Phys. Rev.* **126** 1453
[19] Keski-Rahkonen O and Krause M O 1974 *At. Data Nucl. Data Tables* **14** 139
[20] Kuzmin A, Purans J, Benfatto M and Natoli C R 1993 *Phys. Rev.* B **47** 2480
[21] Dalba G, Fornasini P, Kuzmin A, Purans J and Rocca F 1994 *to be published*
[22] Morinaga M, Sato K, Harada J, Adachi H, Ohba S and Saito Y 1983 *J. Phys. C: Solid State Phys.* **4** L177